[8]Reilly, J. P., Ballantyne, A., and Woodroffe, J. A., "Modeling of Momentum Transfer to a Surface by Laser Supported Absorption Waves," *AIAA Journal*, Vol. 17, No. 10, 1979, pp. 1098–1105.

[9]Simons, G. A., "Momentum Transfer to a Surface When Irradiated by a High-Power Laser," *AIAA Journal*, Vol. 22, No. 3, 1984, pp. 1275–1280.

[10]Sedov, L. I., *Similarity and Dimensional Methods in Mechanics*, Academic Press, New York, 1959.

[11]Katsurayama, H., Komurasaki, K., Momozawa, A., and Arakawa, Y., "Numerical and Engine Cycle Analyses of a Pulse Laser Ramjet Vehicle," *Transaction of JSASS Space Technology*, Vol. 1, No. 1, 2003, pp. 9–16.

N. Gatsonis
Associate Editor

Prolonged Payload Rendezvous Using a Tether Actuator Mass

Paul Williams* and Chris Blanksby†
Royal Melbourne Institute of Technology, Bundoora, Victoria 3083, Australia

Nomenclature

L = tether reference length, km
l = tether length, km
m_1 = actuator mass, kg
m_2 = tether tip mass, kg
N = degree of Lagrange polynomial
R = orbit radius, km
T = tether tension, N
u = nondimensional control tension
θ = in-plane tether libration angle, rad
Λ = nondimensional tether length, l/L
ν_p = angle of payload relative to rendezvous position, rad
ν_s = angle of mother satellite relative to rendezvous position, rad
Π = actuator mass ratio, m_1/m_2
ω = orbital angular velocity of mother satellite, rad/s

Subscripts

p = payload
s = mother satellite
1 = actuator mass
2 = tether tip

Superscripts

$\cdot$ = differentiation with respect to time, $\mathrm{d}(\,)/\mathrm{d}t$
$'$ = differentiation with respect to nondimensional time, $\mathrm{d}(\,)/\mathrm{d}(\omega t)$

Introduction

SPACE tethers have been proposed for a wide range of useful applications.[1] Some of the most promising applications of tether technology involve momentum-exchange techniques. The extreme length of tethered space structures combined with the high strength and low mass of tether materials makes momentum-exchange technology a very efficient means of space transportation. Previous research has demonstrated that significant mass savings can be achieved by utilizing tether technology compared to conventional propellant systems.[2,3] Some of the more exciting momentum-exchange applications include transfer from low Earth orbit (LEO) to destinations such as the moon or Mars. Such exciting applications have been examined in some detail in Refs. 4 and 5. Other promising applications include the capture and subsequent deorbit of inoperational satellites or other space debris.[6]

Tether-mediated rendezvous has been studied previously by Stuart,[7] as well as Blanksby and Trivailo[8] for the in-plane case. Unlike traditional spacecraft rendezvous, tether-mediated rendezvous means that the target payload and mother satellite are in different orbits. Thus there might be a very short rendezvous window during which the payload and capture device are in close proximity, making capture extremely difficult.

Blanksby et al.[9] have obtained minimum reel-rate rendezvous trajectories including the case in which the orbits of all masses are not coplanar. It is probably not practical to achieve instantaneous rendezvous using current technology, as is typically required in tethered momentum transfer applications. Stuart[7] has considered this problem and proposed releasing the tether tension when the tip of the tether matches the position and velocity of the payload, thereby allowing the tether tip to more or less follow the target orbit. Corrections could be achieved using thrusters at the tether tip. However, from a practical viewpoint this is not a very desirable solution because 1) it requires propellant to be replenished at the subsatellite, 2) firing thrusters during proximity with the payload could endanger the payload, and 3) recovering control of the tether from zero or near zero tension could prove difficult. In an effort to circumvent some of these difficulties, Blanksby and Trivailo[8] considered using an additional mass that crawls along the tether to help improve the controllability of the tether tip and to extend the rendezvous window. In their work, a predictive controller was used to control the three-mass system during the rendezvous maneuver. In this Note, we consider a similar configuration and will refer to the tether crawler as an actuator mass (AM). The rendezvous maneuver is formulated as an optimal control problem and solved using a Legendre pseudospectral method. Previously, Blanksby and Trivailo[8] considered capture only at the tether tip using such a system. However, in this Note we will consider capture at both the tether tip and the actuator mass.

Equations of Motion

The assumptions used in the derivation of the equations of motion are as follows: 1) the main spacecraft (mother satellite) is sufficiently large in mass so that center of mass of the system can be assumed to coincide with the mother satellite, 2) the mother satellite is in an unperturbed circular orbit, 3) only the in-plane motion of the system is considered, 4) the system masses are considered as points masses, and 5) the tether masses are neglected. Note that in reality the center of mass will shift as the mass distribution changes, and this in turn influences the orbital motion. This coupling is neglected here but should be included in future analysis of the concepts discussed in this Note. Although only in-plane motion is studied here, perturbations will inevitably cause out-of-plane motion in the system. It is assumed that these are controlled by an appropriate means, such as tether reeling or thrusters, prior to initiating the controller for prolonging rendezvous.

Consider the jth subsatellite of mass m_j connected to the $(j-1)$th subsatellite via the jth tether, as indicated in Fig. 1a. In this Note, m_1 refers to the AM, and m_2 refers to the tether tip, as shown in Fig. 1a. The equations of motion are defined in a rotating (x, y) coordinate system, centered at C on the mother satellite. The x axis points positively outward along the orbit radius vector, and the y axis points along the orbital direction. The equations of motion including the effect of a linearized gravity gradient can be derived via Newton's second law and written as follows:

$$\ddot{x}_j - 2\omega\dot{y}_j - 3\omega^2 x_j = \frac{\left(\sum F_x\right)_j}{m_j} \tag{1}$$

Received 27 October 2003; revision received 8 March 2004; accepted for publication 1 June 2004.

*Ph.D. Candidate, School of Aerospace, Mechanical, and Manufacturing Engineering, P.O. Box 71; tethers@hotmail.com. Student Member AIAA.

†Senior Research Fellow, School of Aerospace, Mechanical, and Manufacturing Engineering, P.O. Box 71; chris.blanksby@rmit.edu.au.

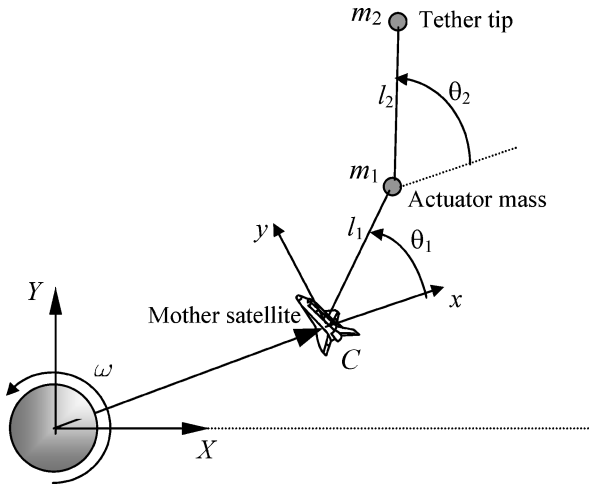

Fig. 1a Simplified representation of tether actuator mass system.

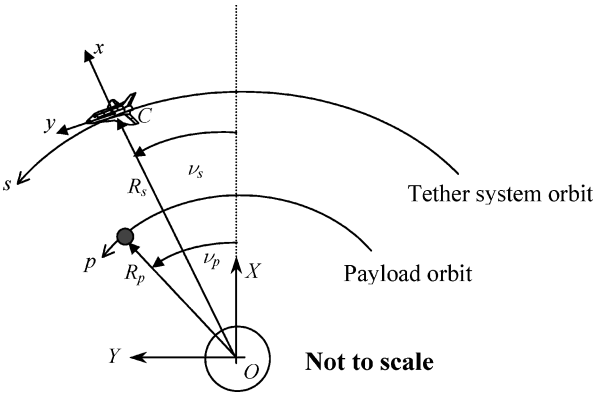

Fig. 1b Parameters and coordinates used for prolonged rendezvous calculations.

$$\ddot{y}_j + 2\omega\dot{x}_j = \frac{\left(\sum F_y\right)_j}{m_j} \tag{2}$$

where F_x and F_y represent the external forces excluding gravity in the x and y directions, respectively. The generalized coordinates for the jth subsatellite, as shown in Fig. 1a, are selected as the tether length l_j and in-plane libration angle θ_j. The Cartesian coordinates are related to these generalized coordinates as follows:

$$x_j = \sum_{k=1}^{j} l_k \cos\theta_k \tag{3}$$

$$y_j = \sum_{k=1}^{j} l_k \sin\theta_k \tag{4}$$

The tension forces acting on each subsatellite can be determined as

$$\sum_j \boldsymbol{F}_j := \begin{cases} \boldsymbol{T}_{j+1} - \boldsymbol{T}_j, & 1 \le j < n \\ -\boldsymbol{T}_n, & j = n \end{cases} \tag{5}$$

where the jth tension force is defined by

$$\mathbf{T}_j = T_j(\cos\theta_j \boldsymbol{i} + \sin\theta_j \boldsymbol{j}) \tag{6}$$

Substitution of Eqs. (3–6) into Eqs. (1) and (2) gives the governing equations for the system. The resulting equations of motion for $n = 2$ can be written in nondimensional form as follows:

$$\theta_1'' = -2(\theta_1' + 1)(\Lambda_1'/\Lambda_1) - 3\sin\theta_1\cos\theta_1 - (u_2/\Lambda_1)\sin(\theta_1 - \theta_2) \tag{7}$$

$$\Lambda_1'' = \Lambda_1\left[(\theta_1' + 1)^2 + 3\cos^2\theta_1 - 1\right] - u_1 + u_2\cos(\theta_1 - \theta_2) \tag{8}$$

$$\theta_2'' = -2(\theta_2' + 1)(\Lambda_2'/\Lambda_2) - 3\sin\theta_2\cos\theta_2 + (u_1/\Lambda_2)\sin(\theta_1 - \theta_2) \tag{9}$$

$$\Lambda_2'' = \Lambda_2\left[(\theta_2' + 1)^2 + 3\cos^2\theta_2 - 1\right] - u_2(1 + \Pi) + u_1\cos(\theta_1 - \theta_2) \tag{10}$$

where $(\,)' = \mathrm{d}/\mathrm{d}(\omega t)$, $\Pi = m_1/m_2$ is the actuator mass ratio, $\Lambda_j = l_j/L$, where L is a reference segment length, and $u_j = T_j/(m_1\omega^2 L)$ is the nondimensional control tension in segment j.

Optimal Rendezvous Problem

Prolonged rendezvous with the target payload is considered for two separate cases: 1) capture at the tether tip and 2) capture at the actuator mass. We focus only on the case of prolonged rendezvous when both the tether platform and payload are in coplanar circular orbits. For prolonged rendezvous, it is necessary to match the position and velocity of the capture point to the position and velocity of the payload over an extended period. Consider the system configuration shown in Fig. 1b. An inertial (rendezvous) coordinate system is introduced and attached to the center of the Earth, $O(OXY)$. This axis system is defined such that the X axis points along the line where the payload and tether platform cross at the same time. The tether dynamics are described in a local orbiting coordinate system (Cxy), attached to the center of mass of the orbiting tether platform. The space tether platform is in a circular orbit of radius R_s, and its position is defined by the angle ν_s measured relative to the X axis (Fig. 1b). The payload is in a circular orbit of radius R_p, and its position is defined by the angle ν_p, also measured relative to the X axis (Fig. 1b). If the independent time variable is selected as ν_s, then ν_p is directly related to ν_s via astrodynamics by

$$\nu_p = (R_s/R_p)^{\frac{3}{2}}\nu_s \tag{11}$$

Equation (11) is derived on the basis that rendezvous for the instantaneous capture case ideally occurs at $\nu_s = \nu_p = 0$. That is, the payload and tether platform both cross the X axis at the same instant, and capture occurs with the tether(s) aligned with the local vertical. For the prolonged rendezvous maneuver a rendezvous window $\nu_s \in [\nu_0, \nu_f]$, which includes $\nu_s = 0$, is assumed with no constraint as to when rendezvous should occur. The inertial positions of the payload (X_p, Y_p) and tether platform (X_s, Y_s) are given, respectively, as

$$X_p = R_p\cos\nu_p, \qquad Y_p = R_p\sin\nu_p \tag{12}$$

$$X_s = R_s\cos\nu_s, \qquad Y_s = R_s\sin\nu_s \tag{13}$$

The inertial position of the capture point (X_c, Y_c) is related to the orbital coordinates of the capture point (x, y) as follows:

$$\begin{Bmatrix} X_c \\ Y_c \end{Bmatrix} = \begin{Bmatrix} X_s \\ Y_s \end{Bmatrix} + \begin{bmatrix} \cos\nu_s & -\sin\nu_s \\ \sin\nu_s & \cos\nu_s \end{bmatrix} \begin{Bmatrix} x \\ y \end{Bmatrix} \tag{14}$$

For capture at the tether tip,

$$X_c^{\mathrm{tip}} = (R_s - l_1\cos\theta_1 - l_2\cos\theta_2)\cos\nu_s + (l_1\sin\theta_1 + l_2\sin\theta_2)\sin\nu_s$$

$$Y_c^{\mathrm{tip}} = (R_s - l_1\cos\theta_1 - l_2\cos\theta_2)\sin\nu_s + (l_1\sin\theta_1 + l_2\sin\theta_2)\cos\nu_s \tag{15}$$

For capture at the actuator mass,

$$X_c^{\mathrm{AM}} = (R_s - l_1\cos\theta_1)\cos\nu_s + l_1\sin\theta_1\sin\nu_s$$

$$Y_c^{\mathrm{AM}} = (R_s - l_1\cos\theta_1)\sin\nu_s + l_1\sin\theta_1\cos\nu_s \tag{16}$$

For prolonged rendezvous, we seek to minimize the distance between the capture point and the payload during the rendezvous window. Equivalently, the control task is to find the control tensions u_1 and u_2 that minimize the cost function

$$\mathcal{J} = \int_{\nu_0}^{\nu_f} \left[(X_p - X_c)^2 + (Y_p - Y_c)^2\right] \mathrm{d}\nu \tag{17}$$

subject to the dynamical equations (7–10), the control inequalities

$$0.001 \le u_1 \le 200, \qquad 0.001 \le u_2 \le 200 \tag{18}$$

and the initial conditions

$$\theta_1 = \theta_2, \qquad \theta_1' = \theta_2', \qquad \Lambda_1' = \Lambda_2' = 0 \tag{19}$$

Note that the units for the control tension are nondimensional. The control limits are set to avoid extremely large spikes in the tether tension that could lead to severance and to restrict the tether from compression, which is not physically realizable.

Capture Hardware

There can be many possible configurations for an actuator mass system and many alternative capture devices. One such conceptual design is shown in Fig. 2. The capture device is a high-strength capture net and cushioned bag. The capture bag has an additional supporting structure to control attitude and possibly position errors. One tether is proposed to be reeled from a spool on the mother satellite, and the second tether is proposed to be reeled from a second spool located on the actuator mass. This allows the two tether lengths to be controlled independently with tension control, rather than having to deal with the complex interaction of a crawler-type mechanism sliding along the tether.

Overview of Numerical Solution Method

In this Note the Legendre pseudospectral method[10] is used to solve the optimal control problem defined by Eqs. (17–19). In this method, the states and controls are approximated discretely by Nth-order Lagrange interpolating polynomials. The $N+1$ nodes used for discretization are defined as the Legendre–Gauss–Lobatto points, which are the extrema of an Nth-order Legendre polynomial in the interval $[-1, 1]$ including the endpoints. The state equations are approximated by analytically differentiating the interpolating polynomial and forcing it to be equal to the state equations at the collocation points by a set of equality constraints. The differentiation can be performed efficiently by way of a differentiation matrix. The integral performance index is approximated using an Nth-order Gauss–Lobatto quadrature rule. The discretization of the original problem leads to a nonlinear programming formulation that can be solved using existing algorithms such as NPSOL.[11] The method is more fully described in Ref. 10.

Numerical Results and Discussion

The optimal rendezvous problem is solved using $N = 50$ with the initial guess generated by integrating the equations of motion with fixed length tether segments. The tether platform is assumed to be in an orbit of radius $R_s = 6870$ km, and the payload is assumed to be in an orbit of radius $R_p = 6770$ km. The reference length of each tether segment is chosen as $L = 50$ km, and the subsatellite mass ratio is set to be $m_1/m_2 = 0.66$. The reference length should be chosen so that the problem is well scaled. Ideally, L should be 100 km for capture at the actuator mass; however, $L = 50$ km is employed for consistency between the two capture cases. This ensures that the scaling of the control tension is the same for both cases. Note also that the ratio m_1/m_2 is selected arbitrarily and could be used as an optimization parameter or varied systematically to gauge its affect on the prolonged rendezvous scenario. The rendezvous window is selected to be the interval $\nu_s \in [-0.5, 0.5]$ rad. This is equivalent to approximately 15 min in real time. This is quite a long period, and it is expected that varying the length of this interval will produce different results. This is an avenue for additional research.

Numerical results are presented in Figs. 3–6. Figure 3 shows the proximity of the payload to the capture point for both capture at the tether tip and capture at the actuator mass. This illustrates that capture at the actuator mass is two orders of magnitude more effective at prolonging rendezvous than capture at the tether tip. In fact, capture at the tether tip gives proximity with the payload of approximately 40 m on three occasions in a 9-min interval, whereas capture at the actuator mass gives proximity of less than 1 m for over 9.5 min. Figure 4 shows the tension control inputs in the tether segments required to maintain close proximity with the payload. Figure 4a shows the tension in tether 1, and Fig. 4b shows tension in tether 2. Capture at the tether tip can be seen to be undesirable from a practical point of view because tension in the lower segment is set to the lower limit for nearly the entire rendezvous interval. Capture at the actuator mass provides a more desirable control input for the tether tensions because the tension is sufficiently above the lower limit for most of the rendezvous interval. Comparison of the tension plots for the two cases shows that the tensions in the two segments differ significantly for capture at the tether tip, with significant peaks in the tension in segment 1, whereas the tensions are virtually identical

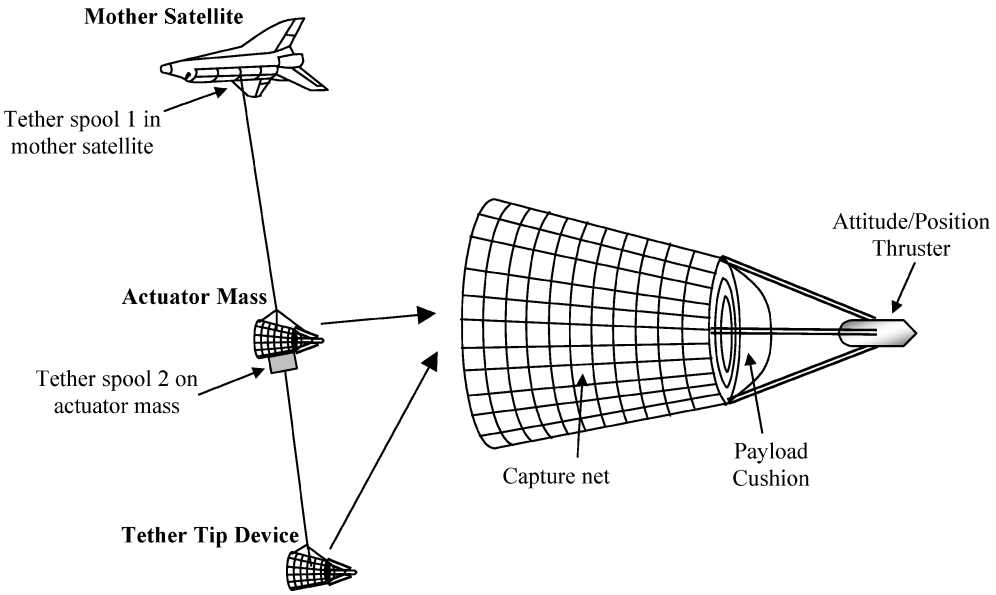

Fig. 2 Possible capture configuration with actuator mass.

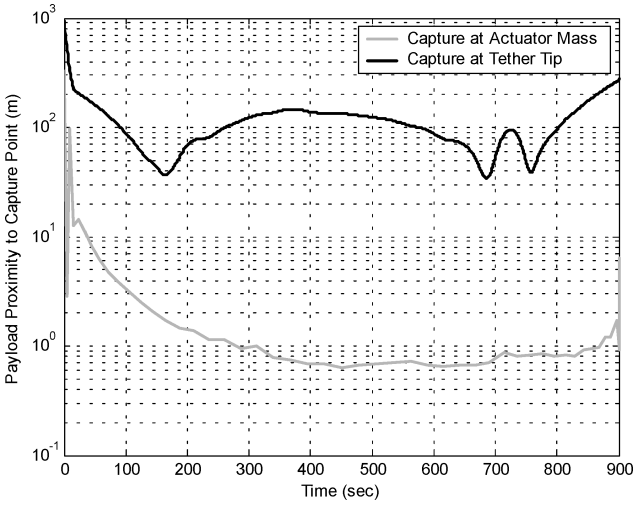

Fig. 3 Proximity of the payload to capture point during prolonged rendezvous using actuator mass configuration.

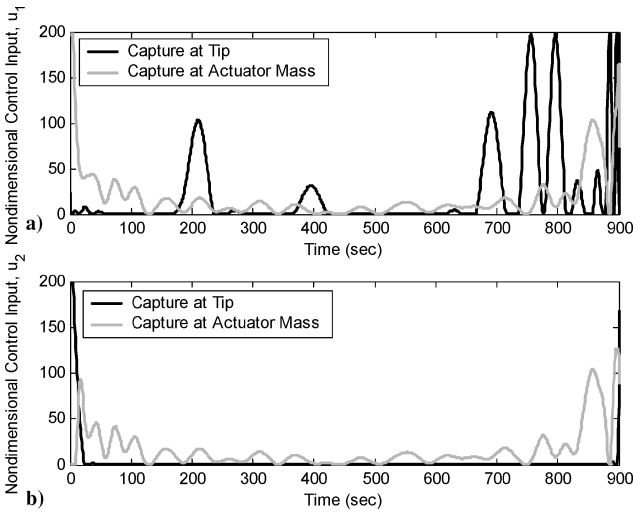

Fig. 4 Nondimensional tension control inputs required to maintain close proximity with payload using an actuator mass configuration.

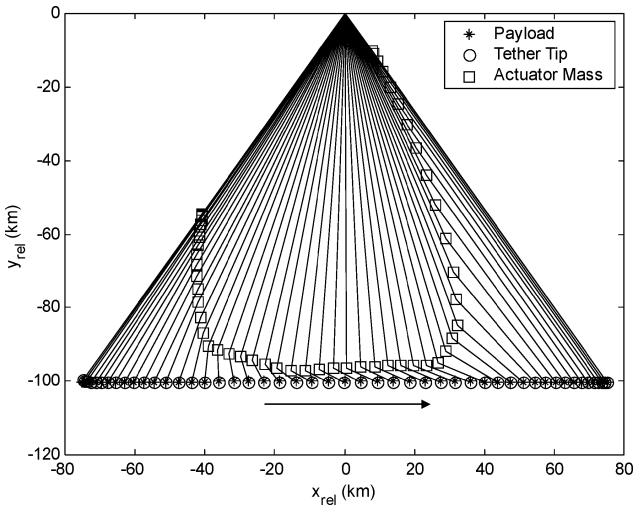

Fig. 5 Projections of tether positions relative to tether platform in orbital coordinates for capture at the tether tip.

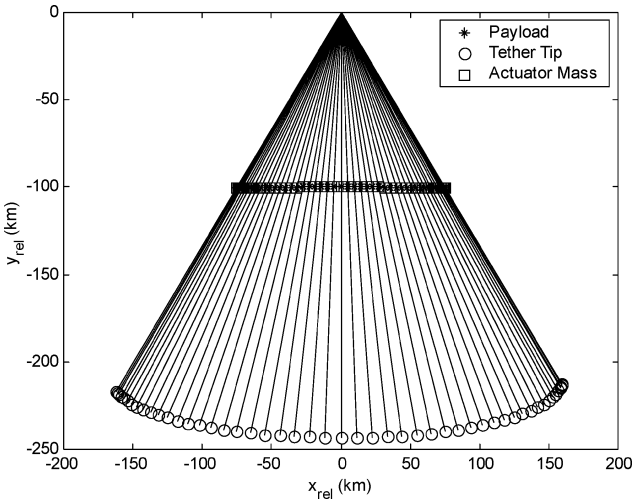

Fig. 6 Projections of tether positions relative to tether platform in orbital coordinates for capture at the actuator mass.

in the case of capture at the actuator mass. Figures 5 and 6 show projections of the tether orientations with respect to the tether platform during rendezvous. Figure 5 shows that capture at the tether tip requires some significant variation in the position of the actuator mass to maintain proximity with the payload. It can also be seen that there are some significant differences in the segment angles, which could be dangerous in terms of initiating high-order tether vibrations or significant out-of-plane effects. Figure 6 shows that capture at the actuator mass produces a very smooth and relatively small variation in the position of the actuator mass. It is also shows that for optimal proximity the lower tether segment needs to be about 1.5 times the length of the upper segment. This increases the total length of tether required from approximately 100 to 250 km, which is certainly a nontrivial increase. It might be possible to reduce the total length by placing additional constraints on the lengths of segments, but this can reduce the rendezvous time. This is certainly an area that could be pursued in future work. Another important factor to consider is the tether length rate requirements. Capture at the tip requires unrealistic reel rates of over 200 m/s, whereas capture at the actuator mass requires reel rates of between 50 and 60 m/s during the time when the payload is in close proximity. These requirements could be reduced by shortening the rendezvous window or allowing some freedom in the initial length rates. Overall, for the scenario considered here, it is evident that capture at the actuator mass is the most desirable option for prolonged rendezvous.

Conclusions

The possibility of prolonging tether-assisted rendezvous with a target payload by using an actuator mass was considered. It was shown that an additional mass can be used to prolong the proximity of the payload with the capture point. Numerical results suggest that capture at the actuator mass can provide a relatively long period (on the order of 9 min) in which the payload and capture point are in close proximity. When using an actuator mass, this appears to be preferable to capturing the payload at the tip because of the larger tension in the tether segments as well as lower length rate requirements. Further study of the effects of the rendezvous window and actuator mass ratio on the dynamics should be undertaken, as well as comparisons with the case where no actuator mass is used.

References

[1]Carroll, J. A., "Tether Applications in Space Transportation," *Acta Astronautica*, Vol. 13, No. 4, 1986, pp. 165–174.

[2]Longuski, J. M., Puig-Suari, J., and Mechalas, J., "Aerobraking Tethers for the Exploration of the Solar System," *Acta Astronautica*, Vol. 35, No. 2/3, 1995, pp. 205–214.

[3]Williams, P., Blanksby, C., and Trivailo, P., "Tethered Planetary Capture Maneuvers," *Journal of Spacecraft and Rockets*, Vol. 41, No. 4, 2004, pp. 603–613.

[4]Tethers Unlimited, Inc., "Cislunar Tether Transport System," Univs. Space Research Association, Final Rept. on NIAC Phase I Contract 07600-011 with NASA Inst. for Advanced Concepts, Clinton, WA, May 1999.

[5]Tethers Unlimited, Inc., "Moon and Mars Orbiting Spinning Tether Transport Architecture Study," Univs. Space Research Association, Final Rept. on NIAC Phase II Contract 07600-034 with NASA Inst. for Advanced Concepts, Lynwood, WA, Aug. 2001.

[6]Nigjeh, B. K., Blanksby, C., and Trivailo, P., "Post-Capture Scenarios for Space Tether Missions," International Astronautical Congress, Paper IAC-02-A.5.03, Aug. 2002.

[7]Stuart, D. G., "Guidance and Control for Cooperative Tether-Mediated Orbital Rendezvous," *Journal of Guidance, Control, and Dynamics*, Vol. 13, No. 6, 1990, pp. 1102–1108.

[8]Blanksby, C., and Trivailo, P., "Assessment of Actuation Methods for Manipulating Tip Position of Long Tethers," *Space Technology*, Vol. 20, No. 1, 2000, pp. 31–39.

[9]Blanksby, C., Williams, P., and Trivailo, P., "Tether Assisted Rendezvous for Satellites with Small Relative Inclinations," International Astronautical Congress, Paper IAC-03-A.P.09, Sept.–Oct. 2003.

[10]Ross, I. M., and Fahroo, F., "Legendre Pseudospectral Approximations of Optimal Control Problems," *Lecture Notes in Control and Information Sciences*, Vol. 295, edited by W. Kang, M. Xiao, and C. Borges, Springer-Verlag, Berlin, 2003, pp. 327–342.

[11]Gill, P. E., Murray, W., Saunders, M. A., and Wright, M. A., "User's Guide to NPSOL 5.0: A Fortran Package for Nonlinear Programming," Stanford Optimization Lab., Stanford Univ., TR SOL 86-1, Stanford, CA, July 1998.

I. Vas
Associate Editor

Skin-Friction Prediction for High-Speed Turbulent Boundary Layers with Ablation

Yichuan Fang* and William W. Liou†
Western Michigan University, Kalamazoo, Michigan 49008
and
Shuxuan Xu‡
University of Science and Technology of China, 230026 Hefei, Anhui, People's Republic of China

Introduction

DEVELOPMENT of advanced high-speed missiles and reentry aerospace vehicles has prompted continued research in aerothermodynamics with increased emphasis on accurate predictions of their aerodynamic performance. In such applications, the effects of surface ablation have received considerable attention. Inherent in the ablation process is surface erosion and accompanying development of surface roughness and mass blowing. Surface roughness generally causes augmentation of the skin friction over aerodynamic surfaces, whereas blowing causes a reduction. In an ablation process, these two phenomena interact and their combined effects on skin friction are not well understood.

Presented as Paper 2003-1250 at the AIAA 41st Aerospace Sciences Meeting, Reno, NV, 6–9 January 2003; received 25 February 2004; revision received 10 May 2004; accepted for publication 10 May 2004.

*Research Associate, Department of Mechanical and Aeronautical Engineering.

†Professor, Department of Mechanics and Mechanical Engineering.

‡Professor, Department of Mechanics and Mechanical Engineering; currently retired.

The effects of surface roughness on skin friction have been examined in many experiments and numerical calculations. Since Nikuradse's[1] work on sand-grain pipe flows, experiments on roughness effects have been reported.[1–4] The effects of roughness have been considered based on the standard of sand-grain roughness initially proposed by Schlichting.[2] Roughness elements were analyzed using equivalent sand-grain roughness. Many studies on the effects of mass blowing on skin friction have been reported for a wide range of flow speeds. The effects of molecular weight of the blowing gas, wall temperature, flow Mach number, angle of attack, and boundary-layer transition were addressed in various investigations.[5–8] The experimental results do not always match and, in some cases, the disagreement is quite significant. Lin et al.[9] contributed a large scattering of experimental data on effects of transverse curvature, pressure gradient, flow being not fully turbulent, different wall temperature ratios, Mach numbers, and how gases were injected from the surface. Jeromin[10] and Laganelli et al.[7] also pointed out that the effects of blowing on skin friction become more significant as the Mach number increases.

Many numerical simulations of ablation[11–14] have been reported recently. Issues related to the design of thermal protection systems (TPSs) for spacecraft and hypersonic reentry vehicles were examined by considering the thermal response of the material and mass injection. The surface roughness effects of ablation, especially on the skin friction and other aerodynamic variables, are not reported.

There are currently no theoretical analyses that can be used to evaluate skin friction under the combined influence of roughness and blowing. Voisinet[15] and Holden[16] reported experimental studies on the combined effect. Based on experimental observations, Voisinet[15] suggested a functional relationship to couple roughness effects to those of mass blowing. Laganelli and Sontowski[17] proposed a method that includes the effect of pressure gradient to predict skin friction with coupled roughness and blowing.

Inspired by the work of Laganelli and Sontowski[17] and the experimental findings of Voisinet,[15] we have developed a new computational methodology to calculate the combined effects of roughness and blowing on skin friction. The two-step approach involves iterative calculation of skin friction with roughness and a second explicit calculation using the information obtained in the previous step. The results of skin-friction calculations for a supersonic turbulent boundary layer over a flat plate will be presented and the results will be compared with available experimental data.

Technical Approach

Effect of Roughness on Skin Friction

Goddard[18] proposed a correlation of the form

$$c_f^{o/r} \Big/ c_f^{o/o} = f(\lg Re_k) \tag{1}$$

to account for roughness effects on skin friction for adiabatic no-blowing walls. The superscripts o/r and o/o represent without-blowing/with-roughness and without-blowing/without-roughness, respectively. Also,

$$Re_k = u_\tau k_s/\upsilon_w, \qquad u_\tau = u_e\sqrt{\left(c_f^{o/r}\Big/2\right)(\rho_e/\rho_w)} \tag{2}$$

k_s denotes the equivalent sand-grain roughness height. The functional form in Eq. (1) was not explicitly given in Goddard. A comparison with data (Fig. 27 in Goddard[18]), however, showed satisfactory agreement. Nestler[19] replotted Goddard's results using the logarithm to the base 10 of a roughness Reynolds number and included the effects of wall cooling.

In this study, a correlation has been developed to fit the data in Fig. 27 of Goddard.[18] The new correlation can be written as

$$c_f^{o/r} \Big/ c_f^{o/o} = 1 + 0.889[0.365(T_w/T_r) + 0.635] \times \left(\lg Re_k - \lg Re_k^c\right)\left(Re_k > Re_k^c\right) \tag{3}$$

Re_k^c represents a critical roughness Reynolds number, below which the skin friction is assumed not to be affected by the surface